Int. J. Heat Mass Transfer. Vol. 12, pp. 1281–1293. Pergamon Press 1969. Printed in Great Britain

THE EFFECT OF PERIODIC SHOCK-FRONTED PRESSURE WAVES ON INSTANTANEOUS HEAT FLUX RATES

R. W. GOLUBA† and G. L. BORMAN‡

Department of Mechanical Engineering, The University of Wisconsin, Madison, Wisconsin

(*Received* 3 *September* 1968 *and in revised form* 19 *March* 1969)

Abstract—Instantaneous heat flux rates were measured at the end-wall of a tube in which shock-fronted, longitudinal pressure waves were generated. Pressure oscillations with frequencies of 479–881 Hz, amplitudes up to 175 psi peak-to-peak, and average tube pressures from 40 to 190 psia were obtained. The heat flux was calculated from the surface temperature of the end-wall as measured by a thin platinum resistance film deposited on a Pyrex surface inserted into the end-wall.

The instantaneous heat flux was found to be large compared to the time-average heat transfer rate. The instantaneous rates increased with increasing pressure ratio and were proportional to the square root of the product of the wave frequency and the time-averaged pressure of the oscillations.

A one-dimensional model was solved numerically for the case of zero net heat transfer to the end-wall. The calculations agreed with the experimentally observed trends and correctly predicted the shape of the periodic portion of the flux.

NOMENCLATURE

- c_p, specific heat at constant pressure;
- f, frequency;
- k, thermal conductivity;
- l, thermal boundary layer thickness;
- p, pressure;
- p_0, pressure at reference condition;
- $\bar{p}$, time-averaged pressure;
- q_w, periodic portion of heat flux;
- Q^*, positive portion of heat transferred per cycle;
- r, radial distance from tube center-line;
- t, time;
- t_0, period of pressure wave;
- T, absolute temperature;
- T_0, absolute temperature at reference condition;
- u, velocity;
- x, distance from end-wall surface;
- y, dimensionless temperature;
- z, dimensionless distance;
- Δz, finite difference increment in z;
- z_l, dimensionless distance to outer boundary condition.

Greek symbols

- α_0, thermal diffusivity;
- γ, ratio of specific heats;
- δ, distance parameter;
- ρ, density;
- ρ_0, density at reference condition;
- τ, dimensionless time;
- $\Delta\tau$, finite difference increment in τ;
- τ^*, fraction of cycle period during which periodic heat flux is positive.

INTRODUCTION

IN STUDIES of rocket engine oscillatory combustion it is important to understand the coupling mechanism between large amplitude pressure waves and the heat-mass transfer

† This paper is based on a thesis submitted by R. W. Goluba, who is presently at the Lawrence Radiation Lab. Livermore, California, in partial fulfilment for the degree of Doctor of Philosophy at the University of Wisconsin. The research was conducted under the sponsorship of the National Aeronautics and Space Administration, Grant No. NsG 601.

‡ Associated Professor of Mechanical Engineering, University of Wisconsin.

process at the gas-fuel interface [1]. In addition, it is of interest to understand the mechanism by which such waves cause the large observed increases in heat transfer to the metal surfaces of the combustor. This paper is aimed at providing information on the latter question with the hope that it may also provide a starting point for similar heat-mass transfer studies.

The current study thus places primary emphasis on experimentally obtaining instantaneous rates of heat transfer and explaining the mechanism causing the observed behaviour. To be of most use in rocket engine studies steep-fronted pressure waves of large amplitude and frequencies greater than 500 Hz were used.

The direction of wave travel relative to the heat transfer surface is of great importance in determining the heat-transfer mechanism. If the direction of wave travel is parallel to the surface the gas velocity profile plays a dominant role. If the direction of wave travel is perpendicular to the surface the compression and expansion process becomes the important mechanism. For the case of waves traveling parallel to the surface, numerous studies of time-average heat-transfer rates for flows in tubes and over flat plates have been reported [2–10]. While some of the laminar flow cases have been mathematically modeled, the studies with large amplitude waves and in particular with steep-fronted waves [7] give data which are difficult to model because the basic mechanism is related to the turbulent scrubbing action of the waves.

For the case of waves traveling normal to the surface, instantaneous rates have been reported by Wendland [11] and Levy and Potter [12]. Wendland used a piston in cylinder apparatus to generate pressure oscillations and measured the instantaneous heat flux at the cylinder head. Ideally his experiment should have yielded a bulk compression and expansion of the gas and a one-dimensional flow normal to the transfer surface. While his data have limited applicability to rocket studies because of the frequency range (10–60 Hz) and the sinusoidal shape of the pressure variations they do show that the heat-transfer phenomena may be modeled with some success by use of laminar flow equations. Levy and Potter measured the instantaneous heat flux at the end-wall of a rarefaction wave tube. Because the heat flux was unidirectional during the initial expansion, periodic effects could not be determined. It is nevertheless important to note that these data could again be successfully explained by using one-dimensional laminar flow models [12, 13].

In setting up the experiments reported here it was felt that periodic waves impinging normal to the surface might provide data amenable to mathematical analysis if the measurements could be taken in a stagnation region where the flow would be essentially one-dimensional. Experiments were thus performed in which instantaneous heat flux was measured at the center of the end-wall of a tube in which longitudinal pressure waves were generated. The apparatus was designed to generate shock-fronted waves of amplitudes up to 175 psi, shock pressure ratios of 1·5–3·2 and frequencies from 479 to 881 Hz. The experimental results were then compared to an unsteady one-dimensional laminar flow model.

EXPERIMENTAL APPARATUS

The experimental apparatus that was used to generate the periodic shock-fronted pressure waves is shown schematically in Fig. 1. The pressure waves were generated by periodically interrupting the inlet air flow to a resonant tube by means of a rotating disk. The disk is 23 in. dia. with eighteen 0·75 in. dia. holes equally spaced at a radius of 8·6 in. The disk was rotated at three different speeds so that pressure waves at frequencies of 479, 694, and 881 Hz were generated. The operation of the apparatus is much like that of a shock tube in that the disk suddenly exposes air at a high inlet pressure to air at a lower pressure, generating a shock of moderate strength. The disk then shuts off the air supply for a short time before reopening.

The air flow was bled from the periphery of the tube through a thin gap maintained between the

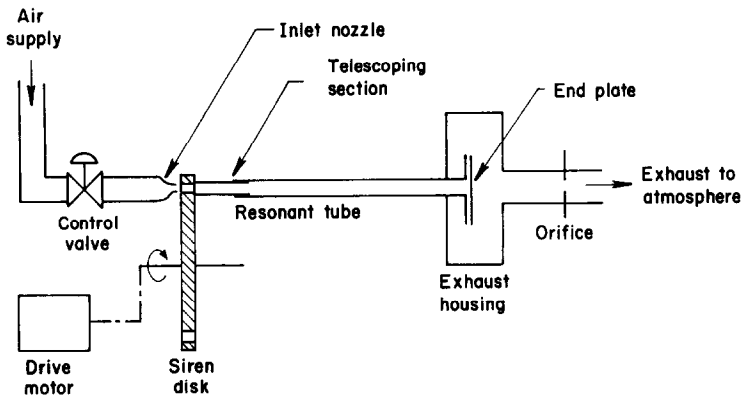

FIG. 1. Schematic diagram of the experimental apparatus.

open end of the tube and a flat plate located perpendicular to the tube axis. This plate forms the end-wall on which the instantaneous heat flux was measured.

The tube, 0·968 in. internal diameter and made of brass, could be adjusted to a resonant length through the use of a telescoping section which provides for a continuous adjustment of up to 1·25 in. and by tube spacers for incremental changes in length. At the resonant length the tube acts as if it were an organ pipe closed at both ends.

The location of the instrumentation as installed at the test section is shown in Fig. 2. The instantaneous pressure was measured by a Kistler 601L pressure transducer located 0·5 in. upstream from the end-plate. Because of the wave reflections from the end-plate, the pressure oscillation measured by this upstream probe exhibits a step which is not present at the end-

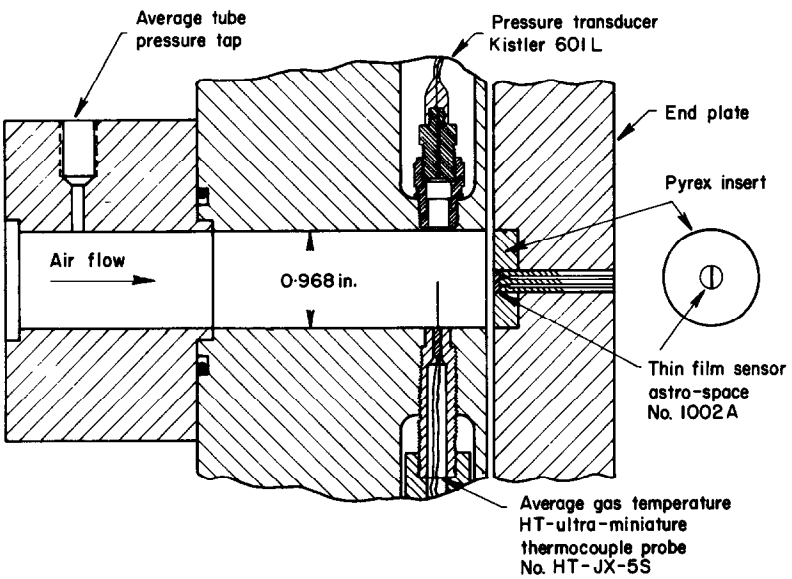

FIG. 2. Test section instrumentation.

plate. Simultaneous measurements of the pressure wave at the two locations are shown in Fig. 3. Comparison of the two pressure waves shows that the shape of the pressure wave at the end-plate can be obtained by extrapolation from the pressure measurement made 0·5 in. upstream. The extrapolation of the pressure wave is shown in Fig. 4 by the dashed line. In

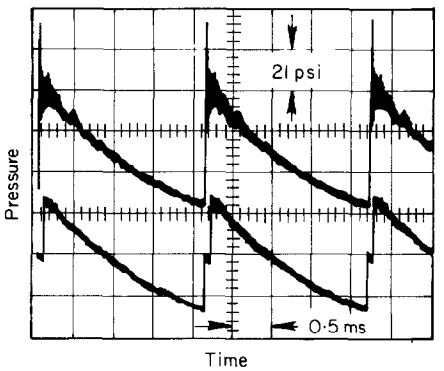

FIG. 3. Experimental pressure oscillations measured at the end-plate (upper trace) and 0·5 in. upstream (lower trace).

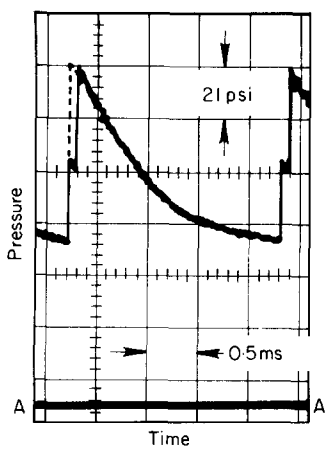

FIG. 4. Experimental pressure data measured 0·5 in. from end-plate with extrapolation shown as dashed line. Line *A–A* is the atmospheric pressure reference line.

this manner the absolute value of the instantaneous gas pressure was obtained. The amplitude of the pressure wave varied from 23 to 182 psi with resulting pressure ratios across the wave of 1·50–3·19.

To obtain measurable surface temperature oscillations, it was necessary to use a low thermal conductivity end-wall surface—thereby minimizing the thermal penetration depth. A Pyrex disk, 1·0 in. dia. by 0·25 in. thick, was inserted in the end-plate as shown in Fig. 2. The surface temperature oscillation was measured by a thin platinum film (1000 Å thick) deposited at the center of the Pyrex disk. The thin film, 0·02 in. wide by 0·19 in. long and with a 10 μs rise time, was placed in a Wheatstone bridge circuit and operated as a resistance thermometer. In this manner, surface temperature oscillations, as shown in Fig. 5, were obtained at amplitudes of 0·25–2·25°F. Extrapolation of the surface temperature signal as shown in Fig. 5 was necessary

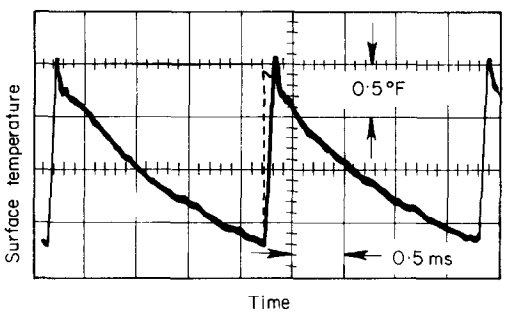

FIG. 5. Experimental surface temperature oscillations with extrapolation shown as dashed line.

because the rise time of the low noise amplifier used was larger than that of the surface temperature. By use of an amplifier with an improved rise time, but with an unacceptable noise level, the surface temperature rise time was determined to be than of the platinum thin film (10 μs).

The periodic heat flux at the Pyrex–gas interface was calculated by solving the one-dimensional unsteady heat transfer equation using an implicit finite difference method. The periodic temperature variation at the Pyrex-gas boundary was obtained from the resistance film data. The Pyrex temperature at a distance of 0·062 in. from the gas side surface was obtained from an imbedded thermocouple. Calcu-

lations show that the temperature oscillations penetrate to a distance of less than 0·01 in. from the surface. Thus the thermocouple at 0·062 in. measures a constant temperature. Because the heat conduction equation is linear (assuming constant thermal conductivity of the Pyrex) the solution could be divided into a steady-state component and an unsteady, periodic component. If the gas side surface is held at the time-average of the measured surface temperature and the temperature at 0·062 in. is held at the value obtained from the thermocouple the steady-state heat flux will result. The periodic component is obtained if the gas side surface is equal to the periodic measured surface temperature and the temperature at 0·062 in. is held at the time-average of the gas side surface value. The time-average of the periodic flux component will of course then be zero.

Unfortunately, the measured values of steady (net) heat flux could not be accurately obtained because the average temperature difference was less than 3°F with an error of ± 1°F. The values of experimental heat flux, q_w, reported here are thus restricted to the fluctuating component only. The steady flux was estimated to be from 10 to 30 per cent of the time-average of the absolute value of the fluctuating component of the flux.

Figure 6 shows a typical set of data for pressure, surface temperature, and calculated heat flux. As can be seen, the pressure and temperature traces are both steep-fronted with no measurable phase difference between the pressure and temperature fronts.

An average gas temperature (90–100°F and only a few degrees higher than the average surface temperatures of the Pyrex) was measured 0·5 in. upstream from the end-plate by a fine wire thermocouple supported by a 0·008 in. dia. stainless steel sheath. Average mass flow rates of air through the tube from 0·13 to 0·49 lbm/s were measured by a thin plate orifice after the air was discharged from the end of the tube and at a point where the flow oscillations were negligible.

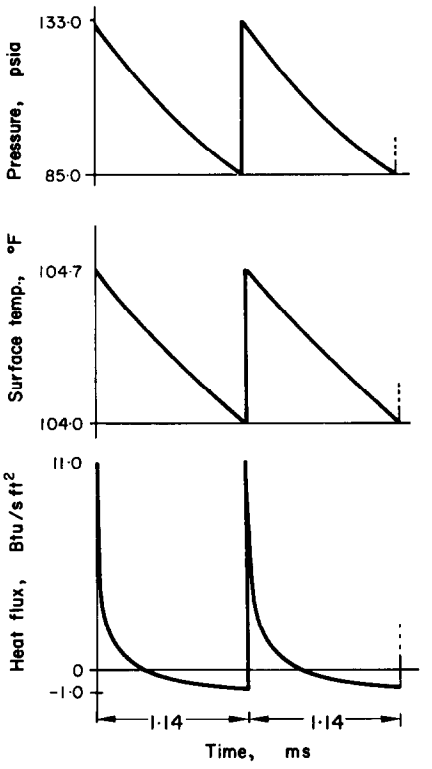

FIG. 6. Typical set of pressure, surface temperature, and heat flux data.

THEORY

Before discussing the experimental results, it is important to obtain an understanding of the boundary layer phenomena which govern the correlations. To obtain such an understanding, a theoretical model was developed for the thermal boundary layer at the center of the end-wall.

Figure 7 shows the coordinates and air flow direction for the heat transfer test section. From flow visualization studies using a surface oil technique and from tests with various plate gaps, it was inferred that the flow near the plate surface at $r = 0$ was essentially one-dimensional and in the x direction. It was thus assumed that a one-dimensional model could be used to predict the boundary layer phenomena at the center of the end-plate.

In order to simplify the model, it was assumed

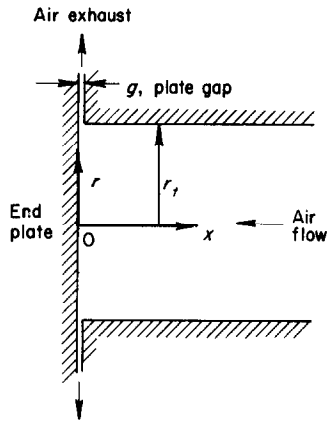

FIG. 7. Test section coordinates.

that the pressure variation through the boundary layer could be neglected making the pressure a function of time only. With this assumption the momentum equation need not be solved if the pressure variation with time is supplied from experimental data. This assumption should be valid if the boundary layer is thin and if the temperature gradients within the boundary layer are not too large. For large temperature gradients which would result from large pressure ratios, the effect of the $\partial p/\partial x$ term in the energy equation would not necessarily be negligible.

Assuming a thin boundary layer with moderate temperature variations, the effects of turbulence and variations of thermal conductivity and specific heat ratio were neglected. With these assumptions and neglecting viscous dissipation, the energy equation for an ideal gas is given by

$$\frac{\gamma p}{T(\gamma - 1)}\frac{\partial T}{\partial t} + u\frac{\partial T}{\partial x} = \frac{\mathrm{d}p}{\mathrm{d}t} + k\frac{\partial^2 T}{\partial x^2}. \quad (1)$$

Because the measured surface temperature of the end-plate never fluctuated more than 2°F, it was assumed constant relative to the gas temperature variation. Thus, the boundary condition at $x = 0$ is given by

$$T(0, t) = T_w \quad (2)$$

where the surface temperature, T_w, is a specified constant. Because the measured net heat flux per cycle to the end-plate was small compared to the variation during the cycle, it will be assumed zero so that the gas outside the boundary layer can be considered to be undergoing an isentropic process, if viscous effects can be neglected. Defining l as the time varying thickness of the thermal boundary layer, the boundary condition at $x \geqslant l$ is then given by

$$T(l, t) = T_0(p/p_0)^{(\gamma - 1)/\gamma} \quad (3)$$

where p_0 and T_0 are reference values arbitrarily taken here to be the values corresponding to the minimum pressure during the cycle.

Since the steady periodic solution is desired, the initial condition is replaced by

$$T(x, t) = T(x, t + t_0) \quad (4)$$

where t_0 is the period of the cycle.

In order to solve equation (1), an expression for the velocity, u, must be obtained from a solution of the continuity equation. An approximate expression for u can be obtained by assuming that the density is independent of x in the continuity equation and is equal to the gas density at $x = l$. Using this approximation and the boundary condition $u(0, t) = 0$, the velocity distribution is given by

$$u(x, t) = -x\frac{\mathrm{d}p}{\mathrm{d}t}/(\gamma p). \quad (5)$$

The accuracy of this approximate expression for the velocity will be discussed toward the end of this section.

The governing equations are now recast in terms of the following dimensionless variables;

$$y = T(x, t)/T(l, t) \quad (6)$$

$$z = x/\delta(t) \quad (7)$$

$$\tau = t/t_0 \quad (8)$$

where

$$\delta(t) = (\alpha_0 t_0)^{\frac{1}{2}} (p/p_0)^{-1/\gamma}$$

and

$$\alpha_0 = k/(c_p \rho_0) = T_0(\gamma - 1)k/(\gamma p_0).$$

Substituting these variables into equations (1) and (5) and combining gives

$$\frac{1}{y}\frac{\partial y}{\partial \tau} = \left(\frac{p}{p_0}\right)^{1/\gamma} \frac{\partial^2 y}{\partial z^2}. \tag{9}$$

Equations (2)–(4) become

$$y(0, \tau) = T_w/T(l, \tau) \tag{10}$$

$$y(z_l, \tau) = 1 \tag{11}$$

$$y(z, \tau) = y(z, \tau + 1) \tag{12}$$

where $z_l \geqslant l(t)/\delta(t)$.

Equations (9)–(12) can be solved numerically if T_w, t_0 and p/p_0 are supplied from experimental data. The finite difference predictor-corrector method of Douglas and Jones [14] was used to obtain the numerical solution. With an increment size of $\Delta z = 0{\cdot}055$, stable solutions were obtained with $\Delta\tau = 0{\cdot}001$ for $0 \leqslant \tau \leqslant 0{\cdot}05$ and $\Delta\tau \leqslant 0{\cdot}003$ for $0{\cdot}05 \leqslant \tau \leqslant 1{\cdot}0$. Using this increment size, the rise time of the shock-front was 2·1 μs for a wave frequency of 479 Hz. This rise time approximates the rise time which was experimentally estimated. For all of the calculated results presented here, z_l was taken to be 2·75 which was found to be large enough to be outside the thermal boundary layer for all cases considered. For the range of variables used, the boundary-layer thickness was never greater than 0·02 in. This is small as compared to the wave length of the pressure oscillation which is 2·3 ft at 479 Hz.

Because of the assumptions used in obtaining equations (3) and (5), the net energy exchange per cycle at the boundary $z = z_l$ must be zero. Therefore, the model can only be used for cases where the net heat transfer at $x = 0$ is negligible To be consistent with the model, T_0 must be chosen so that the net amount of heat transferred to the wall per cycle is zero. The value of T_0 required to meet this condition was obtained by iteration. The first trial value of T_0 was obtained from

$$T_0 = T_w / \int_0^1 (p/p_0)^{(\gamma-1)/\gamma} \, d\tau. \tag{13}$$

The thermal conductivity of the air was held constant and evaluated at the wall temperature, T_w. From the resulting solution it was found that the conductivity deviation from that at the wall was 25 per cent for the most extreme case and less than 10 per cent for the majority of calculations.

Figure 8 shows a typical set of dimensionless gas temperature profiles and Fig. 9 shows the

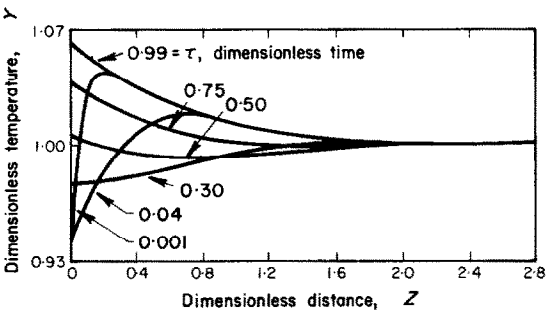

FIG. 8. Calculated y vs. z profiles: frequency, 881 Hz; tube pressure, 105 psia; pressure ratio for wave front, 1·56. Experimental pressure corresponds to that given in Fig. 6.

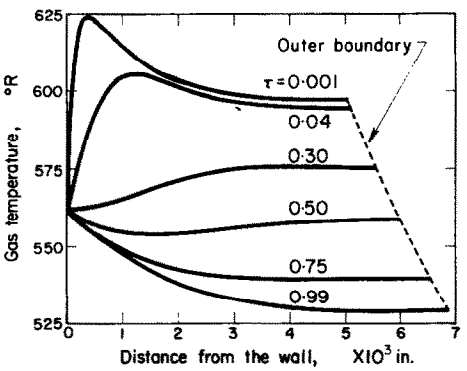

FIG. 9. Calculated gas temperature profiles corresponding to the dimensionless profiles of Fig. 8.

dimensional profiles for the same data. At the end of the cycle ($\tau = 0{\cdot}99$), the gas temperature decreases monotonically from the wall value and asymptotically approaches the isentropic value at the outer edge of the boundary layer. When the shock-front arrives ($\tau = 0{\cdot}001$), the pressure work causes a steep temperature gradient at the wall with a temperature maximum within the boundary layer (at $x = 0{\cdot}0003$ in. for the data of Fig. 9). As the expansion process continues, the temperature gradient at the wall decreases and eventually changes sign. During the expansion process a temperature profile of the shape shown in Fig. 10 occurs. For such a

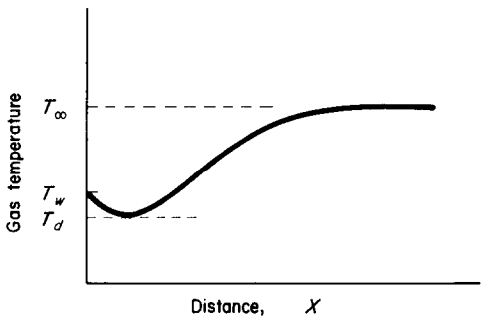

FIG. 10. Shape of gas temperature profile which results in a negative heat transfer coefficient.

profile the heat flux is from the wall to the gas ($T_w > T_d$) although the gas temperature at the outer edge of the boundary layer is larger than the wall temperature ($T_\infty > T_w$). A conventional heat transfer coefficient based on the temperature difference ($T_\infty - T_w$) would be negative for such a profile. It is interesting to note that such anomalous coefficient values have been observed in motored combustion engines [15].

From the profiles shown in Fig. 9, it is obvious that sizable density gradients are present in the gas immediately after the arrival of the wave front. These gradients were neglected in obtaining the expression for u so that the approximate velocity given by equation (5) is in error for $\tau \sim 0$. By using the previously calculated temperature profiles and the continuity equation in the form

$$u(x, t) = -\frac{1}{\rho(x, t)} \int_0^x \frac{\partial \rho}{\partial t} dx \qquad (1)$$

corrected values of u were obtained. These calculations showed that equation (5) is a good approximation for $\tau > 0{\cdot}05$ but is a poor approximation for $0 \leqslant \tau \leqslant 0{\cdot}04$. A comparison of the magnitude of the terms $\partial T/\partial t$ and $u\,\partial T/\partial x$ showed, however, that even for $\tau = 0{\cdot}001$, there is only a small region in the boundary layer where these terms are of the same order of magnitude—outside this region $u\,\partial T/\partial x$ is at least an order of magnitude smaller than $\partial T/\partial t$.

In summary, the theory presented applies to the experimental conditions studied—namely, moderate pressure ratios (1·5–3·2) and small net heat transfer. As will be seen in the next section, the calculated results agree reasonably well with the experimental data. To extend the theory to larger pressure ratios or large net heat transfer, it is probable that a number of assumptions would have to be eliminated. In particular, the continuity equation should be solved simultaneously with the energy equation and the thermal conductivity should not be considered constant. Inclusion of the $\partial p/\partial x$ term in the energy equation would greatly complicate the analysis, but may be necessary for very large pressure ratios or very large differences between the wall and average gas temperature.

COMPARISONS OF THEORETICAL AND EXPERIMENTAL DATA

Instantaneous values of gas pressure, surface temperature and heat flux were experimentally obtained for frequencies of 479, 694, and 881 Hz, average tube pressures of 40, 102, and 190 psia and pressure ratios ranging from 1·5 to 3·19. To obtain a given set of data the frequency and average tube pressure were fixed and the pressure ratio was varied by changing the resonant

length of the tube. Experiments with different mass flow rates ranging from 0·13 to 0·48 lbm/s showed that the mass flow had a negligible influence on the heat flux data. Figures 11–13 show a typical set of data for a fixed frequency and tube pressure.

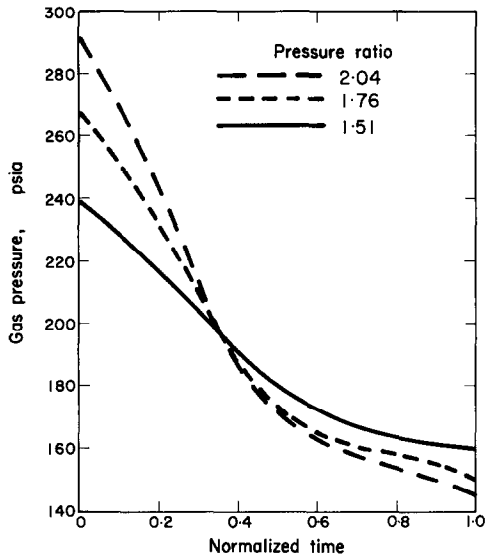

FIG. 11. Experimental gas pressure oscillations: frequency, 479 Hz; tube pressure, 190 psia; mass flow rate, 0·133 lbm/s.

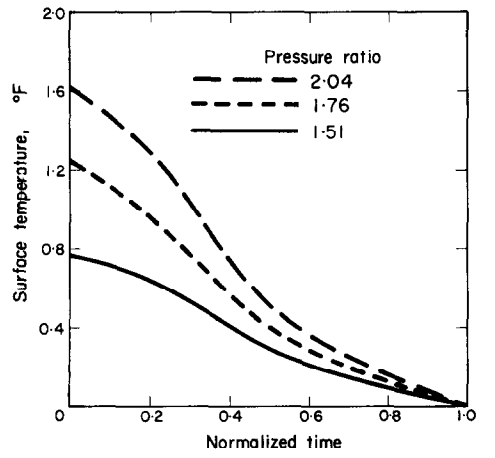

FIG. 12. Experimental surface temperature oscillations, same conditions as data of Fig. 11.

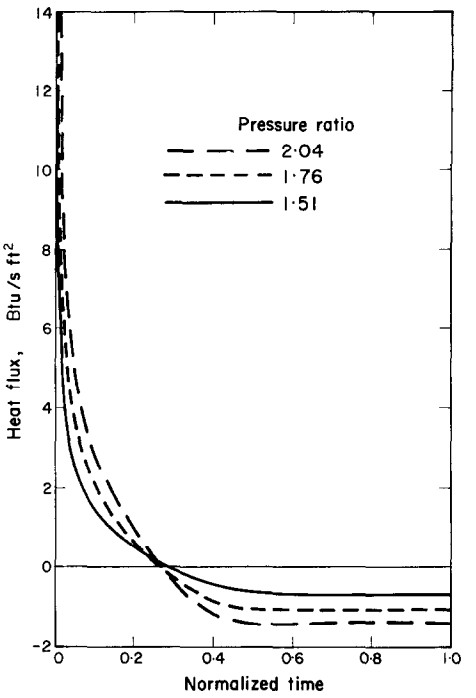

FIG. 13. Experimental heat flux variation, same conditions as data of Fig. 11.

Figure 14 shows a comparison of calculated and experimental heat flux for a typical set of conditions. The theoretical heat flux at the wall surface was calculated from

$$q_w = -T_0 f^{\frac{1}{2}} (k\rho_0 c_p)^{\frac{1}{2}} (p/p_0) \frac{\partial y}{\partial z}\bigg|_{z=0} \qquad (15)$$

where $f = 1/t_0$, the cycle frequency.

It should be remembered that the experimental data shown in Fig. 13 is for the periodic flux only, i.e., the steady-state flux has been subtracted. For the data of Fig. 14, the net flux was estimated to be 0·4 Btu/sft^2 which results in a substantial difference between theory and experiment for the negative heat flux portion of the cycle. The data do show, however, that the correct shape of the instantaneous flux is predicted by

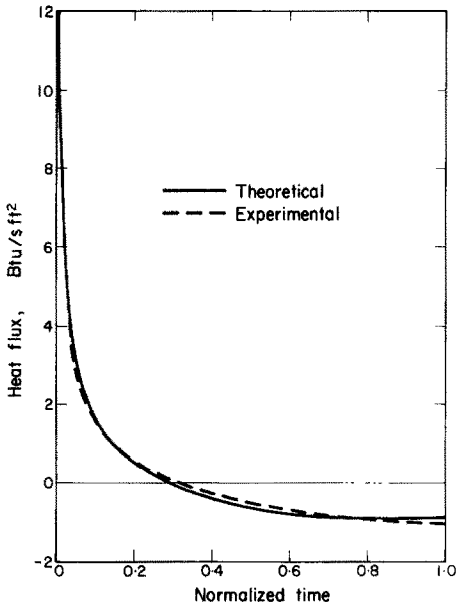

FIG. 14. Comparison of experimental and computed heat flux for the conditions given in Figs. 6 and 8.

the theory. From Fig. 14 it can also be seen that the positive portion of the periodic flux occurs during the first one third of the cycle. This was typical for all of the data obtained. The heat flux at time zero is infinite if the surface temperature is considered to be discontinuous at that point in the cycle. However, the zero time theoretical heat flux was finite because a very small but finite rise time for the pressure wave was used in the finite difference calculations.

In order to compare the theoretical and experimental trends, it is convenient to use a single parameter to characterize the heat flux. The quantity of heat transferred during the positive portion of the periodic flux, Q^*, will be used for this purpose. Thus,

$$Q^* = \frac{1}{f}\int_0^{\tau^*} q_w \, d\tau \qquad (16)$$

where τ^* is the fraction of the cycle period during which heat is transferred from the gas to the wall.

The variation of Q^* with pressure ratio is shown in Figs. 15 and 16 where the solid lines were obtained from the theoretical model. The effect of average tube pressure at a fixed frequency is shown in Fig. 15 and the effect of frequency at a fixed average tube pressure is shown in Fig. 16. For purposes of calculation, the pressure wave shape was held constant along each of the solid lines in these figures. The experimental pressure shapes, however, varied slightly from run to run which accounts for some of the experimental scatter. The agreement between theory and experiment is good except for the 40 psia tube pressure data which lie above the theoretical values. This difference is attributed to a departure from one-dimensional flow which was caused by the large plate gap thickness needed to obtain these conditions.

Using equation (15), it can be shown that if all of the variables except average tube pressure are held constant, then both q_w and Q^* are proportional to the square root of the average tube pressure. Similarly, if all variables except frequency are held constant, then q_w is proportional to and Q^* is inversely proportional to the square root of cycle frequency. The experimental data were found to agree with these predicted trends. Thus, the data of Fig. 17, which give the calculated heat flux distribution for three different pressure ratios, can be used for any frequency, f, and average tube pressure, $\bar{p}$, by multiplying the ordinate values by $[f\bar{p}/(479)(105)]^{\frac{1}{2}}$. It should be noted that in contrast to Fig. 13, the calculated curves of Fig. 17 each correspond to the same normalized pressure wave shape. The shape of the wave used is given in the upper right corner of the figure.

CONCLUSIONS

This investigation has shown that for periodic shock-fronted pressure waves impinging on a plate located normal to the direction of wave travel the instantaneous heat flux from the gas may be quite large, even when the average heat transfer rate is essentially zero. The instantaneous heat flux was found to increase as the square

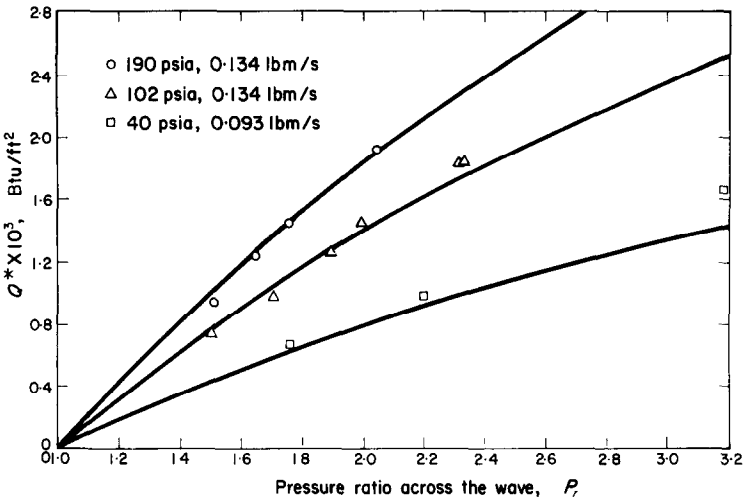

FIG. 15. Positive heat transfer per cycle at three different average tube pressures and a frequency of 479 Hz. Solid lines calculated from theoretical model.

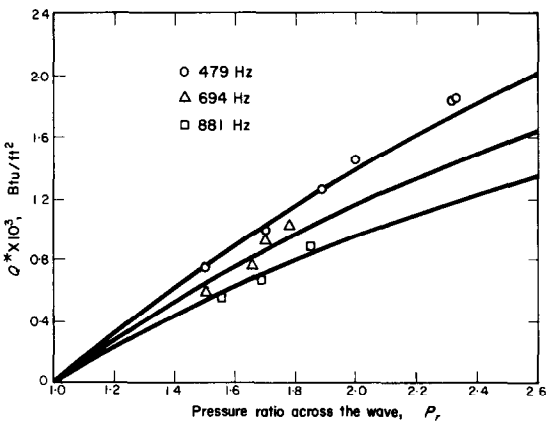

FIG. 16. Positive heat transfer per cycle at three different frequencies with an average tube pressure of 104 psia and a mass flow rate of 0·134 lbm/s. Solid lines calculated from theoretical model.

root of the product of frequency and average pressure. The heat flux also increased with an increase in pressure ratio across the wave. These trends are explained by the rate with which pressure work is done on the gas in the boundary layer. Because the variation in heat flux is large, the analysis of heat transfer in oscillatory pressure environments should

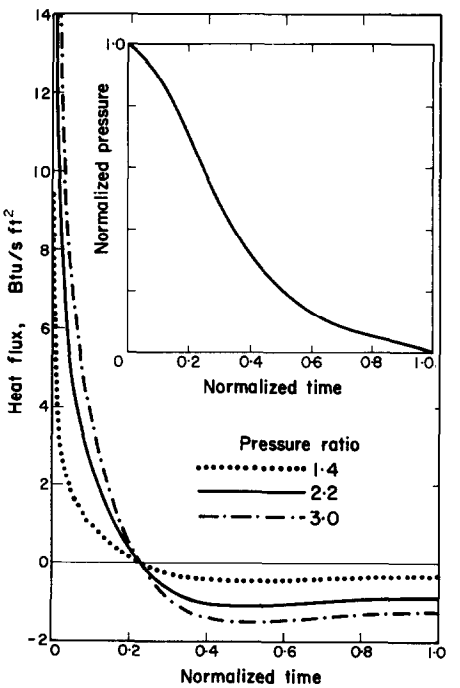

FIG. 17. Calculated heat flux for three pressure ratios: frequency, 479 Hz; average tube pressure, 105 psia. Normalized pressure shape used to obtain each line is shown in upper right corner.

account for the instantaneous rates as well as for the time average rates.

The theoretical model given here shows that the rapid compression of the boundary layer by the arrival of the shock front causes the gas temperature to have a maximum value within the boundary layer a short distance from the wall. This temperature profile causes the large gradient near the wall which results in the observed high instantaneous flux. The model also predicts the experimentally observed trends with pressure ratio, average pressure and frequency. Although the shape of the instantaneous flux is correctly predicted by the model, nonzero average flux rates cannot be determined. Further experimental and theoretical work is thus required to explain the heat-transfer phenomena under conditions of large average heat transfer and large amplitude pressure oscillations.

ACKNOWLEDGEMENTS

The authors wish to thank their colleagues P. S. Myers, O. A. Uyehara and H. G. Weber for their advice and assistance, as well as P. R. Wieber of NASA who acted as contract monitor.

REFERENCES

1. R. J. Priem and D. C. Guentert, Combustion instability limits determined by a non-linear theory and a one-dimensional model, NASA TN D1409 (October 1962).
2. V. Chalitbhan, Effects of longitudinal pulsations on heat transfer, Ph.D. Thesis, University of Texas, January (1959).
3. T. W. Jackson and H. L. Johnson, Convective flow due to acoustic vibrations in horizontal resonant tubes, Georgia Institute of Technology, Final Report, Contract No. Af 49(638)-459, March (1961).
4. T. W. Jackson, K. R. Purdy and C. C. Oliver, The effects of resonant acoustic vibrations on the Nusselt number for a constant temperature horizontal tube, *International Developments in Heat Transfer*, pp. 483–489 (1961–1962).
5. K. R. Purdy, T. W. Jackson and C. W. Gorton, Viscous fluid flow under the influence of a resonant acoustic field, *Trans. Am. Soc. Mech. Engrs. J. Heat Transfer* C, **86**, 97–106 (1964).
6. T. W. Jackson, K. R. Purdy, H. G. Keith and R. S. Rudland, Investigations of the effect of acoustic vibrations on convective heat transfer—final report, Aerospace Research Laboratories Rept. No. ARL 65–97 (1965).
7. D. W. Bodganoff, A study of the mechanisms of heat transfer in oscillating flow, Princeton University Dept. of Aerospace and Mechanical Sciences Technical Report 483f (October 1967).
8. D. T. Harrje, Heat transfer in oscillating flow—final report, Princeton University Dept. of Aerospace and Mechanical Sciences Technical Report 483g, AD664303, (October 1967).
9. F. J. Bayley, P. A. Edwards and P. P. Singh, The effect of flow pulsations on heat transfer by forced convection from a flat plate, *International Developments in Heat Transfer* pp. 499–509 (1961–62).
10. C. E. Feiler and E. B. Yeager, Effects of large-amplitude oscillations on heat transfer, NASA TR-142 (1962).
11. D. W. Wendland, The effects of periodic pressure and temperature fluctuations on unsteady heat transfer in a closed system, Ph.D. Thesis, University of Wisconsin (1968).
12. M. J. Levy and J. H. Potter, Some transient measurements in a rarefaction wave tube, *Trans. Am. Soc. Mech. Engrs, J. Engng. Ind.* B, **86**, 365–370 (1964).
13. B. T. Chao, End wall heat transfer in a rarefaction wave tube, *Trans. Am. Soc. Mech. Engrs. J. Heat Transfer* C, **87**, 349–352 (1965).
14. J. Douglas, Jr. and B. R. Jones, Jr., On predictor-corrector methods for nonlinear parabolic differential equations, *J. Ind. Appl. Math.* **11**, 195 (1963).
15. V. D. Overbye, J. E. Bennethum, O. A. Uyehara and P. S. Myers, Unsteady heat transfer in engines, *S.A.E. Trans.* **69**, 461–494 (1961).

Résumé—Les densités de flux de chaleur instantanées ont été mesurées à la paroi de l'extrémité d'un tube dans lequel des ondes de pressions longitudinales à forme d'ondes de choc étaient produites. Des oscillations de pression avec des fréquences de 479 à 881 Hz, des amplitudes allant jusqu'à 12 bars crête à crête, et des pressions moyennes dans le tube de 2,76 à 13,1 bars ont été obtenues. Le flux de chaleur était calculé à partir de la température de surface de la paroi de l'extrémité mesurée par une résistance constituée par un film fin de platine déposé sur une surface de Pyrex insérée dans la paroi de l'extrémité.

On a trouvé que le flux de chaleur instantané est grand comparé à la densité de flux de chaleur moyénnée dans le temps. Les flux instantanés augmentaient avec le rapport de pression et étaient proportionnels à la racine carrée des produits de la fréquence d l'onde et de la pression moyennée dans le temps des oscillations.

Un modèle unidimensionnel a été résolu numériquement dans le cas d'un flux de chaleur net nul à la paroi de l'extrémité. Les calculs sont en accord avec les tendances observées expérimentalement et prévoient correctement la forme de la portion périodique du flux.

Zusammenfassung—Es wurden augenblickliche Wärmestromdichten am geschlossenen Ende eines Rohres gemessen, in dem man Längsdruckwellen durch stossfronten erzeugte. Die Druckschwingungen hatten Frequenzen von 479 bis 881 Hz und von Spitze zu Spitze gemessene Amplituden von 175 psi bei mittleren Rohrdrücken von 40 bis 190 psia.

Der Wärmestrom wurde aus der Oberflächentemperatur des Rohrendes berechnet, die durch einen dünnen Platin-Widerstandsfilm gemessen wurde, der auf einer in das Rohrende eingeführten Pyrex-Oberfläche aufgebracht war.

Es wurde gefunden, dass der augenblickliche Wärmestrom im Vergleich zum zeitlichen Mittelwert gross ist. Die augenblicklichen Wärmeströme nahmen mit steigendem Druckverhältnis zu und waren proportional zur Wurzel aus dem Produkt aus Wellenfrequenz und zeitlichem Mittelwert der Druckschwingungen.

Für den Fall verschwindenden Gesamtwärmestroms zum Rohrende wurde ein eindimensionales Modell numerisch gelöst. Die Berechnungen stimmten mit den experimentell beobachteten Tendenzen überein und gaben den Verlauf des periodischen Teils des Wärmestroms korrekt wieder.

Аннотация—Измерялся нестационарный тепловой поток на торцовой стенке трубы, на которой генерировались ударные продольные волны давления. Получены колебания давления с частотами 479–881 герц, амплитудой от пика до пика до 175 psi и средним давлением в трубе от 40 до 190 psia. Тепловой поток рассчитывался по температуре поверхности торцовой стенки, которая измерялась пленочным датчиком, вмонтированным в торцовую стенку.

Найдено, что нестационарный тепловой поток больше осредненного по времени. Нестационарный тепловой поток увеличивался с увеличением отношения давления и был пропорционален квадратному корню произведения частоты волны и усредненному по времени давлению.

Одномерная модель рассчитывалась численно для случая нулевого переноса тепла к торцовой стенке. Расчеты согласовывались с экспериментальными наблюдениями и правильно предсказали форму периодической порции потока.